Cite this: *Mater. Chem. Front.*, 2019, **3**, 276

Pairing 1D/2D-conjugation donors/acceptors towards high-performance organic solar cells†

Jiayu Wang,‡[a] Yiqun Xiao,‡[b] Wei Wang,[a] Cenqi Yan,[a] Jeromy Rech,[c] Mingyu Zhang,[a] Wei You,[c] Xinhui Lu*[b] and Xiaowei Zhan*[a]

Received 8th October 2018,
Accepted 10th December 2018

DOI: 10.1039/c8qm00512e

rsc.li/frontiers-materials

Two polymer donors, **FTAZ** and **J71**, and two fused-ring electron acceptors, **ITIC1** and **ITIC2**, are used to investigate the effects of conjugation dimension on the performance of organic solar cells (OSCs). **FTAZ** and **J71**, and **ITIC1** and **ITIC2** share the same molecular backbone, respectively, while **J71** and **ITIC2** possess conjugated thienyl side chains. The addition of conjugated side chains slightly red-shifts the absorption spectra and lowers the bandgap due to the extended 2D conjugation. Conjugated side chains on the acceptor induce the self-aggregation of the acceptors, while conjugated side chains on the donor increase the miscibility of the donors and acceptors, thus optimizing the morphology of the active layers. The blends based on mixed combinations, namely 1D donor/2D acceptor and 2D donor/1D acceptor, show better performance relative to 1D donor/1D acceptor and 2D donor/2D acceptor.

Introduction

Organic solar cells (OSCs) are regarded as a promising alternative to silicon-based photovoltaic technology due to some advantages, such as low cost, light weight, flexibility, semi-transparency, large-area fabrication, and short energy payback times.[1–3] A bulk heterojunction (BHJ) is the most widely used architecture of the active layer in OSCs, which consists of a blend of electron donor and acceptor materials.[4,5] To achieve high power conversion efficiency (PCE), various donors and acceptors have been developed *via* various molecular design strategies, among which two dimensional (2D) conjugated (also called side-chain conjugated) materials exhibit good performance and attract considerable attention. Compared to the nonconjugated counterparts, 2D conjugated side chains can extend intramolecular conjugation, which enhances light absorption and photocurrent. Moreover, 2D conjugation facilitates intermolecular interaction and π–π overlap, thus promoting charge transport.[6,7] During the past decade, a variety of 2D conjugated donors have been developed, which yielded PCEs over 10% in fullerene-based OSCs.[8–10] As for acceptors, Zhan and co-workers introduced the concept of 2D conjugation into fused-ring electron acceptors (FREAs),[11] and a high PCE of 13% was achieved.[12]

Recently, nonfullerene acceptors,[13–16] especially FREAs,[17,18] have attracted much attention and attained high PCEs,[19] but to continue achieving high device performance, it is crucial to keep a balanced partnership between donor and acceptor components in terms of absorption, energy level, mobility, miscibility, and morphology.[20–24] Considering the conjugation dimension of the donor and acceptor, there are four combinations: 1D donor/1D acceptor,[25–32] 1D donor/2D acceptor,[11] 2D donor/1D acceptor,[33–53] and 2D donor/2D acceptor.[12,54] Although various pairs of 1D/2D donor/acceptor have been studied individually, systematic comparisons of 1D/2D donor/acceptor pairs have rarely been reported. These 1D/2D acceptors usually contain different cores and end-groups, and they are often paired with different donor materials to fabricate OSCs, which exhibit different performance, thus leaving the 1D/2D conjugation effect ambiguous. The approach outlined herein aims to properly understand how the 1D/2D conjugation of donor/acceptor would affect device performance and what 1D/2D donor/acceptor combination would be better to achieve higher performance.

In this work, we report the first example of mapping 1D/2D donor/acceptor combinations; specifically we choose two polymer donors, **FTAZ**[55] and **J71**,[35] and two FREAs, **ITIC1**[11] and **ITIC2**[11] (Scheme 1), to systematically compare 1D/2D donor/acceptor pairs. These materials are good candidates for this study as they have each demonstrated high performance, thus allowing the differences associated within to be attributed to the 1D/2D conjugation effect. The donor polymers, **FTAZ** and **J71**, possess the same molecular backbone, but different side

[a] *Department of Materials Science and Engineering, College of Engineering, Key Laboratory of Polymer Chemistry and Physics of Ministry of Education, Peking University, Beijing 100871, China. E-mail: xwzhan@pku.edu.cn*
[b] *Department of Physics, Chinese University of Hong Kong, New Territories 999077, Hong Kong, China. E-mail: xhlu@phy.cuhk.edu.hk*
[c] *University of North Carolina at Chapel Hill, Chapel Hill, North Carolina 27599-3290, USA*

† Electronic supplementary information (ESI) available. See DOI: 10.1039/c8qm00512e

‡ Contributed equally to this work.

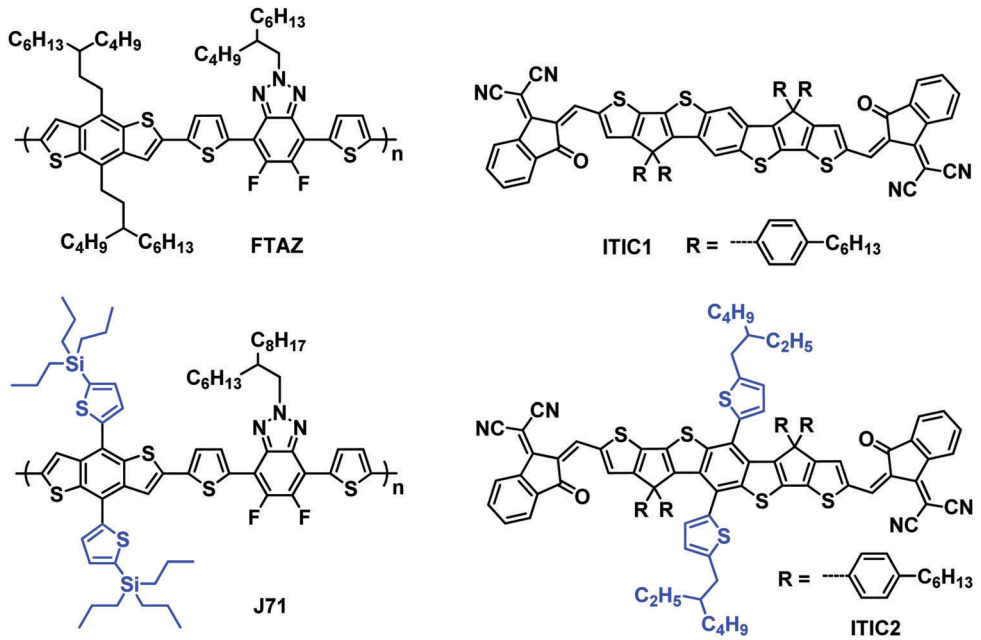

Scheme 1 Chemical structures of **FTAZ**, **J71**, **ITIC1**, and **ITIC2**.

chains on the benzodithiophene units (nonconjugated 3-butylnonyl and conjugated thienyl, respectively). Similarly, the conjugated backbones of acceptors **ITIC1** and **ITIC2** are the same, and the substituents on the central phenyl varied (hydrogen and conjugated thienyl, respectively). Because of the different molecular structures, **FTAZ** and **ITIC1** are characterized by 1D conjugation, while **J71** and **ITIC2** have 2D conjugation. With this small library, we are able to systematically probe the effects of the conjugated side-chains on electronic, optical, charge-transport, morphological and photovoltaic properties of the donors and acceptors. This will allow for a better understanding of the effect of 1D/2D conjugation and help provide recommendations for pairing new materials in the future. The mixed combinations, 1D/2D (**FTAZ:ITIC2**) and 2D/1D (**J71:ITIC1**), show better performance relative to 1D/1D (**FTAZ:ITIC1**) and 2D/2D (**J71:ITIC2**).

Results and discussion

Optical and electronic properties

The optical impact of 1D *vs.* 2D conjugation was first explored with UV-vis absorption. The normalized optical absorption spectra of **FTAZ**, **J71**, **ITIC1**, and **ITIC2** in chloroform and in thin films are shown in Fig. S1a (ESI†) and Fig. 1a, respectively. In solution, the 1D conjugated **FTAZ** shows two peaks at 534 and 572 nm, while 2D conjugated **J71** shows a slightly red-shifted spectrum with two peaks at 536 and 578 nm. The absorption maximum of 1D conjugated acceptor **ITIC1** locates at 702 nm, while that of 2D conjugated **ITIC2** red-shifts to 714 nm. Relative to those in solution, the absorption spectra of **FTAZ** and **J71** in films do not differ much, while those of **ITIC1** and **ITIC2** red-shift. The absorption maxima of 1D conjugated **FTAZ** and **ITIC1** are 533 and 734 nm, respectively; while those of 2D conjugated **J71** and **ITIC2** slightly red-shift to 540 and 738 nm, respectively.

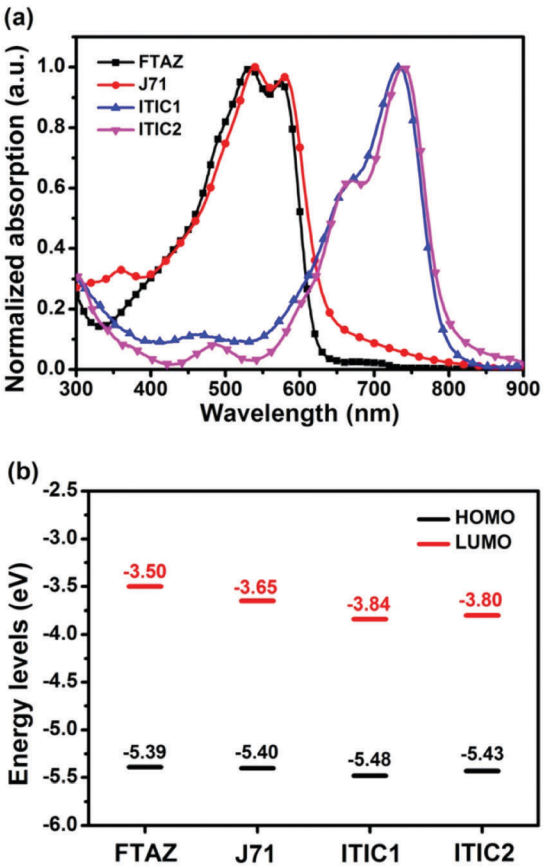

Fig. 1 (a) Thin film UV-vis absorption spectra and (b) energy level diagram from CV of **FTAZ**, **J71**, **ITIC1**, and **ITIC2**.

The increase in absorption maxima in the 2D conjugated systems is attributed to the extended intramolecular conjugation

Table 1 Basic properties of **FTAZ**, **J71**, **ITIC1**, and **ITIC2**

Material	$\lambda^{abs}_{solution}$ (nm)	λ^{abs}_{film} (nm)	E_g[a] (eV)	HOMO (eV)	LUMO (eV)	μ (10^{-3} cm^2 V^{-1} s^{-1})
FTAZ	534, 572	533, 574	2.00	−5.39	−3.50	4.4
J71	536, 578	540, 580	1.96	−5.40	−3.65	3.6
ITIC1	702	734	1.55	−5.48	−3.84	1.0
ITIC2	714	738	1.53	−5.43	−3.80	1.3

[a] Estimated from the absorption edge in film.

from the side chains. The optical bandgaps of **FTAZ**, **J71**, **ITIC1**, and **ITIC2** are estimated from the absorption edge of the thin film: 2.00, 1.96, 1.55, and 1.53 eV, respectively. This information is also found in Table 1. The wide-bandgap polymer donors and low-bandgap acceptors exhibit complementary absorption, which is beneficial for harvesting panchromatic light and improving short-circuit current density (J_{SC}).

Next, the electrochemical properties of **FTAZ**, **J71**, **ITIC1**, and **ITIC2** were investigated by a cyclic voltammetry (CV) method with films on a glassy carbon working electrode in 0.1 M $[^nBu_4N]^+[PF_6]^-$ CH_3CN solution at a potential scan rate of 100 mV s^{-1}. Each of these molecules exhibits irreversible oxidation and reduction waves (Fig. S1b, ESI†). Additionally, the highest occupied molecular orbital (HOMO) and lowest unoccupied molecular orbital (LUMO) energy levels (Fig. 1b and Table 1) were estimated from the onset oxidation and reduction potentials, respectively, assuming the absolute energy level of $FeCp_2^{+/0}$ to be 4.8 eV below vacuum[56] (the oxidation potential of $FeCp_2^{+/0}$ *versus* Ag/AgCl was measured to be 0.45 V). The HOMO energy levels of **FTAZ** (−5.39 eV) and **J71** (−5.40 eV) are similar; while **J71** shows a lower LUMO energy level of −3.65 eV relative to **FTAZ** (−3.50 eV), due to the σ inductive effect of silicon atom.[57] The HOMO and LUMO energy levels of **ITIC1** are −5.48 and −3.84 eV, respectively. **ITIC2** shows slightly higher HOMO and LUMO energy levels of −5.43 and −3.80 eV, respectively, owing to the electron-donating property of thiophene units.

Next, the charge transport properties of these materials are explored. The hole mobilities of **FTAZ** and **J71**, and electron mobilities of **ITIC1** and **ITIC2** in neat films were measured using the space charge limited current (SCLC) method in hole-only (ITO/PEDOT:PSS/**FTAZ** or **J71**/Au) or electron-only (Al/**ITIC1** or **ITIC2**/Al) devices (Fig. S2 (ESI†) and Table 1).[58] The hole mobilities of **FTAZ** and **J71** are 4.4×10^{-3} and 3.6×10^{-3} cm^2 V^{-1} s^{-1}, respectively; the electron mobilities of **ITIC1** and **ITIC2** are 1.0×10^{-3} and 1.3×10^{-3} cm^2 V^{-1} s^{-1}, respectively.

Photovoltaic properties

To further explore the effect of 1D *vs.* 2D conjugation of these materials, BHJ OSCs with the structure of ITO/ZnO/donor: acceptor/MoO_x/Ag were fabricated using **FTAZ** or **J71** as donor and **ITIC1** or **ITIC2** as acceptor. Each of the 4 pairings of donor: acceptor were carefully optimized and the results are summarized in Fig. 2a and Table 2. The optimized **FTAZ:ITIC1**-based devices (*i.e.* 1D/1D) show an open-circuit voltage (V_{OC}) of 0.921 V, J_{SC} of 16.45 mA cm^{-2}, fill factor (FF) of 0.564, and PCE of 8.54%. When switching to a 2D acceptor, **FTAZ:ITIC2**-based devices (1D/2D) exhibit a higher V_{OC} of 0.925 V, higher J_{SC} of 18.88 mA cm^{-2}, higher FF of 0.630, and an overall higher PCE of 11.0%. However, when switching to a 2D donor, **J71:ITIC2**-based devices (2D/2D) exhibit a lower PCE of 9.55% with V_{OC} of 0.940 V, J_{SC} of 16.55 mA cm^{-2}, and FF of 0.614. When moving back to the 1D acceptor, **J71:ITIC1**-based devices (2D/1D) show higher J_{SC}, FF and PCE of 17.90 mA cm^{-2}, 0.653, and 10.6%, respectively. The higher V_{OC} of **ITIC2**-based devices is due to the higher LUMO energy level of **ITIC2** (−3.80 eV compared to −3.84 eV of **ITIC1**). As the HOMO energy levels of **FTAZ** and **J71** are similar, the difference in V_{OC} between **FTAZ** and **J71**-based devices may originate from morphology-induced V_{OC} loss.[59,60] The J_{SC} and FF of mixed combinations 1D/2D and 2D/1D (**FTAZ:ITIC2** and **J71:ITIC1**) are higher than those of 1D/1D (**FTAZ:ITIC1**) and 2D/2D (**J71:ITIC2**) combinations, which leads to higher PCEs.

The external quantum efficiency (EQE) spectra of the optimized devices are shown in Fig. 2b. All of the four EQE spectra exhibit a slight valley at around 600 nm, arising from the separated absorption of donors (400–600 nm) and acceptors (600–800 nm); thus, the donors and acceptors contribute to the photoresponse in the region of 400–600 nm and 600–800 nm, respectively. The J_{SC} of the optimized **FTAZ:ITIC1**, **FTAZ:ITIC2**, **J71:ITIC1**, and **J71:ITIC2** blends calculated from integration of EQE spectra with the AM 1.5G reference spectrum are 15.84, 18.13, 17.59, and 16.50 mA cm^{-2}, respectively, consistent with J_{SC} values measured from *J–V* (the error is <5%, Table 2).

Next, to better understand the differences between the various 1D and 2D pairings, charge recombination in the devices was investigated by measuring V_{OC} (Fig. 2c) and J_{SC} (Fig. 2d) under different incident light intensities (P). The relationship between V_{OC} and P is described by the formula of $V_{OC} \propto \ln P$,[61] where a slope of 1 k_BT/q (k_B: Boltzmann constant, T: temperature, and q: elementary charge) indicates that bimolecular recombination dominates in the device, a slope of 2 k_BT/q indicates that geminate or Shockley–Read–Hall recombination dominates,[62] while a slope of 0.5 k_BT/q indicates that surface recombination dominates.[63,64] The slope for **FTAZ:ITIC1**, **FTAZ:ITIC2**, **J71:ITIC1**, and **J71:ITIC2** blends is 0.99 k_BT/q, 1.02 k_BT/q, 1.04 k_BT/q, and 0.97 k_BT/q, respectively, suggesting that bimolecular recombination dominates in all 4 blends. The relationship between J_{SC} and P is described by the formula of $J_{SC} \propto P^S$, where a value of $S = 1$ indicates that all free carriers are swept out and collected at electrodes before recombination, and $S < 1$ indicates some extent of bimolecular recombination.[65] The S values of **FTAZ:ITIC1**, **FTAZ:ITIC2**, **J71:ITIC1**, and **J71:ITIC2** blends are 0.92, 0.95, 0.94 and 0.93, respectively, indicating relatively weaker bimolecular recombination in mixed combinations 1D/2D and 2D/1D (**FTAZ:ITIC2** and **J71:ITIC1**), which is beneficial for higher FF.

Charge transfer in blended films was investigated by photoluminescence (PL) quenching (Fig. S3, ESI†). **FTAZ** and **J71** are excited at 466 nm and emit at 631 and 636 nm (Fig. S3a, ESI†), respectively; while **ITIC1** and **ITIC2** are excited at 687 nm and emit at 784 and 776 nm (Fig. S3b, ESI†), respectively. According to the absorption spectra of the four materials, excitation at

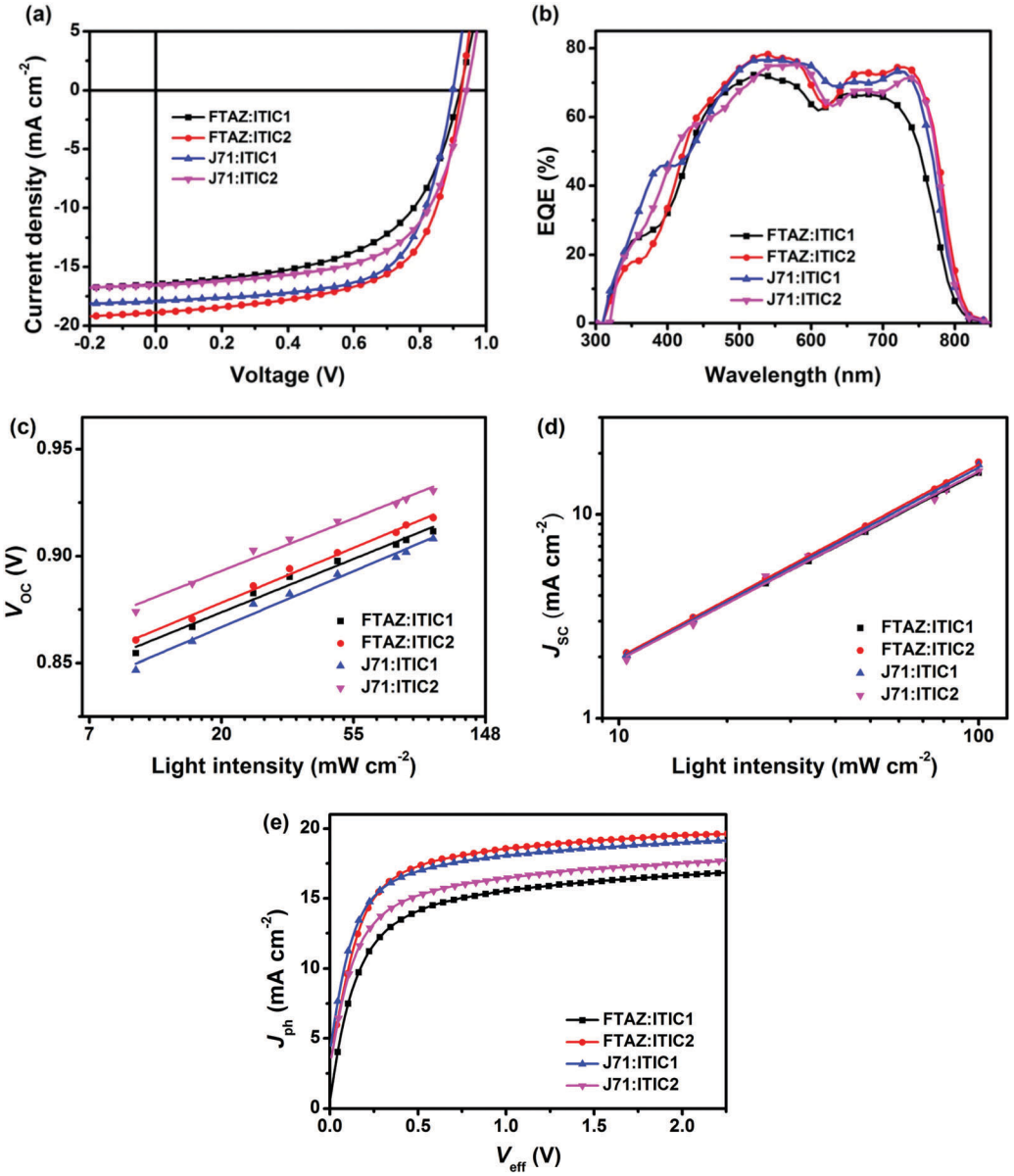

Fig. 2 (a) *J*–*V* curves, (b) EQE spectra, (c) V_{OC} *versus* light intensity, (d) J_{SC} *versus* light intensity, and (e) J_{ph} *versus* V_{eff} of the optimized devices with the structure of ITO/ZnO/active layer/MoO_x/Ag.

Table 2 Performance and mobilities of the optimized devices

Active layer	V_{OC}[a] (V)	J_{SC}[a] (mA cm^{-2})	FF[a]	PCE[a] (%)	Calculated J_{SC} (mA cm^{-2})	μ_h (10^{-4} cm^2 V^{-1} s^{-1})	μ_e (10^{-4} cm^2 V^{-1} s^{-1})	μ_h/μ_e
FTAZ:ITIC1	0.922 ± 0.003 (0.921)	16.06 ± 0.36 (16.45)	0.562 ± 0.004 (0.564)	8.32 ± 0.19 (8.54)	15.84	25	2.0	12.5
FTAZ:ITIC2	0.922 ± 0.003 (0.925)	18.63 ± 0.26 (18.88)	0.620 ± 0.006 (0.630)	10.6 ± 0.2 (11.0)	18.13	12	4.1	2.92
J71:ITIC1	0.908 ± 0.005 (0.911)	17.55 ± 0.23 (17.90)	0.645 ± 0.015 (0.653)	10.2 ± 0.2 (10.6)	17.59	10	3.5	2.85
J71:ITIC2	0.935 ± 0.003 (0.940)	16.29 ± 0.29 (16.55)	0.598 ± 0.014 (0.614)	9.11 ± 0.23 (9.55)	16.50	12	3.7	3.24

[a] Average values with standard deviation were obtained from 20 devices, the values in parentheses are the parameters of the best device.

466 nm mainly excites donors while that at 687 nm mainly excites acceptors. When excited at 466 nm, all of the four blends show over 99% PL quenching, suggesting highly efficient charge transfer from donor to acceptor. When excited at 687 nm, the PL quenching of 1D/2D and 2D/1D, **FTAZ:ITIC2** and **J71:ITIC1**, are 98% and 97%, respectively, slightly higher than that of 1D/1D **FTAZ:ITIC1** (92%) and 2D/2D **J71/ITIC2** (96%), indicating more efficient charge transfer from acceptor to donor, which is beneficial for higher J_{SC}.

Charge generation and extraction efficiencies of these devices were also investigated by measuring the photocurrent

density (J_{ph}) *versus* the effective voltage (V_{eff}) (Fig. 2e).[66] At high V_{eff} (>2 V), all excitons are dissociated into free charge carriers and collected by electrodes, the J_{ph} becomes saturated photocurrent density (J_{sat}), and J_{SC}/J_{sat} characterizes the charge generation and extraction under short-circuit conditions. The J_{SC}/J_{sat} values of mixed combinations 1D/2D and 2D/1D, **FTAZ:ITIC2** and **J71:ITIC1**, are both 94%, higher than that of 1D/1D **FTAZ:ITIC1** (92%) and 2D/2D **J71/ITIC2** (93%). Therefore, the pairings of mixed 1D and 2D materials, compared to 1D/1D or 2D/2D, show more efficient charge generation and extraction, which is beneficial to higher J_{SC} and FF.

Finally, the hole (μ_h) and electron mobilities (μ_e) of the blended films were measured by the SCLC method with device structures of ITO/PEDOT:PSS/active layer/Au for holes (Fig. S4a (ESI†) and Table 2) and Al/active layer/Al for electrons (Fig. S4b (ESI†) and Table 2). The μ_h/μ_e of **FTAZ:ITIC1**, **FTAZ:ITIC2**, **J71:ITIC1**, and **J71:ITIC2** blends are 12.5, 2.92, 2.85, and 3.24, respectively. The 2D/1D system of **J71:ITIC1** shows the most balanced hole/electron transport, which can help explain the highest FF. The unbalanced hole/electron transport in the 1D/1D system of **FTAZ:ITIC1** is responsible for the lowest FF. Both high mobilities and balanced charge transport are needed for high J_{SC} and FF.

Film morphology

While the photovoltaic properties illustrated some of the impact from the various pairings of 1D and 2D conjugated materials, the morphology of each of these blends is also important in elucidating the 1D/2D conjugation effect. Transmission electron microscopy (TEM) was first used to characterize the bulk morphology of the active layers (Fig. S5, ESI†). All of the four blends show relatively uniform morphology without pinholes or large aggregates, which prevents severe recombination. Grazing incidence wide-angle X-ray scattering (GIWAXS) was used to gain more molecular level morphology information.[67] The 2D GIWAXS patterns and the corresponding intensity profiles of the neat donor and acceptor films in the in-plane (q_r) and out-of-plane (q_z) directions are shown in Fig. S6 (ESI†). All four of these materials exhibit a favored face-on orientation in neat films. The lamellar peaks of **FTAZ**, **J71**, **ITIC1**, and **ITIC2** locate at q_r = 0.321, 0.292, 0.333, and 0.299 Å^{-1}, corresponding to *d*-spacings of 19.6, 21.5, 18.9, and 21.0 Å, respectively. The 2D conjugated materials of **J71** and **ITIC2** exhibit larger lamellar *d*-spacings relative to the 1D conjugated counterparts of **FTAZ** and **ITIC1**. The π–π stacking peaks of **FTAZ**, **J71**, **ITIC1**, and **ITIC2** locate at q_z = 1.66, 1.66, 1.79, and 1.85 Å^{-1}, corresponding to *d*-spacings of 3.79, 3.79, 3.51, and 3.40 Å, respectively. While the π–π stacking peaks of **FTAZ** and **J71** are both at 3.79 Å, **FTAZ** shows a larger π–π crystallite coherence length (CCL) of 20.6 Å relative to **J71** (16.2 Å). A larger CCL is beneficial to high mobility, and this difference can help explain the differences in the hole mobilities for the two materials. Additionally, **ITIC1** (13.3 Å) and **ITIC2** (13.2 Å) exhibit similar π–π CCLs, leading to similar electron mobilities in neat films.

Next, the optimized blended films were also investigated, and the 2D GIWAXS patterns and the corresponding intensity profiles of the blended films are presented in Fig. 3. Much like the neat materials, all of the four blended films show a preferential face-on orientation. The lamellar packing peaks of **FTAZ**:acceptor films locate at $q_r \sim 0.330$ Å^{-1} (d = 19.0 Å), while those of **J71**:acceptor blends locate at $q_r \sim 0.310$ Å^{-1} (d = 20.3 Å). **J71**:acceptor blends exhibit larger lamellar *d*-spacings relative to **FTAZ**:acceptor blends, resembling the trend in the neat films of **J71** (2D) and **FTAZ** (1D). The π–π stacking peaks of **FTAZ:ITIC1**,

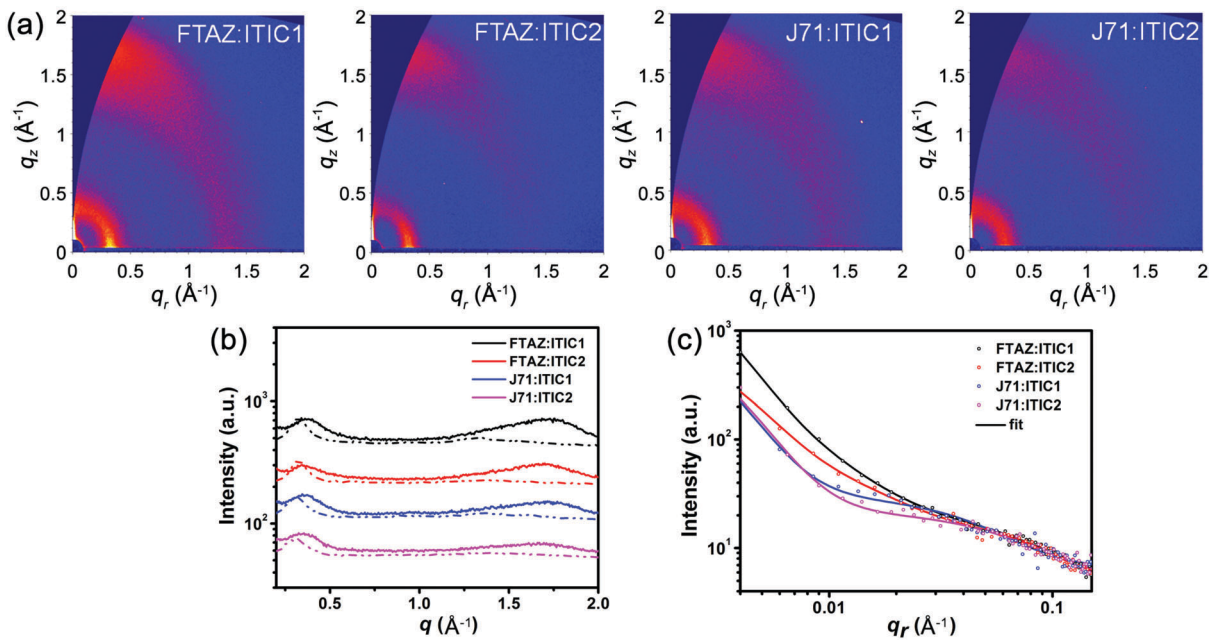

Fig. 3 (a) 2D GIWAXS patterns, (b) GIWAXS intensity profiles along the in-plane (scattered line) and out-of-plane (solid line) directions, and (c) GISAXS intensity profiles and best fittings along the in-plane direction of the optimized active layers.

FTAZ:**ITIC2**, **J71**:**ITIC1**, and **J71**:**ITIC2** blends locate at q_z =1.70, 1.67, 1.69, and 1.66 Å^{-1}, respectively, with CCLs of 7.13, 12.7, 10.5, and 10.1 Å, respectively. The 1D/2D mixed blends show slightly larger CCLs than the 1D/1D and 2D/2D blends, which might contribute to the relatively better device performance results.

Finally, grazing incidence small-angle X-ray scattering (GISAXS) measurements were performed to understand the phase separation information for the various blends. Phase separation, which originates from the miscibility of donor and acceptor, significantly affects the device performance.[68,69] Low miscibility leads to formation of large pure domains, while high miscibility leads to formation of large intermixing domains. Large pure domain is beneficial to charge transport but unfavorable to exciton splitting, while large intermixing domain facilitates exciton splitting but restrains charge transport. Thus it is crucial to solve this paradox by precisely tuning the miscibility of donor and acceptor to reach a balance between exciton splitting and charge transport. The in-plane intensity profiles and the 2D GISAXS patterns of the neat and blended films are presented in Fig. 3c and Fig. S7 (ESI†), respectively. For **FTAZ**:acceptor blended films, we adopt the Debye–Anderson–Brumberger (DAB) model, a polydispersed hard sphere model and a fractal-like network model to account for the scattering contribution from intermixing amorphous phases, **FTAZ** domains and acceptor domains, respectively.[70] For **J71**:acceptor blended films, we adopt the DAB model and a fractal-like network model[70] since the scattering of **J71** is very weak (Fig. S7, ESI†). The **FTAZ** domains retain similar sizes for **FTAZ**:acceptor blends (4.2–4.5 nm). The intermixing domain sizes of **FTAZ**:**ITIC1**, **FTAZ**:**ITIC2**, **J71**:**ITIC1**, and **J71**:**ITIC2** films are 26.2, 24.4, 30.7, and 36.3 nm, respectively, while the acceptor domain sizes are 21.0, 22.0, 5.74, and 7.14 nm, respectively (Table 3). The acceptor domain sizes of the **ITIC2**-based (2D) films are larger than those of **ITIC1**-based (1D) films, suggesting that the conjugated side chains on the acceptor facilitate molecular packing and growth of acceptor domains, which is beneficial for higher electron mobility in blended films. The intermixing domain sizes of **J71**-based (2D) films are also larger than those of **FTAZ**-based (1D) films, indicating that the conjugated side chains on the donor increase the miscibility of the donor and acceptor. However, when mixing the 2D donor of **J71** with the 2D acceptor of **ITIC2**, the film exhibits the largest intermixing domain size, suggesting that the increased miscibility may originate from the interactions between the side chains of the donor and acceptor. Compared to the **FTAZ**:**ITIC1** (1D/1D) system, **FTAZ**:**ITIC2** (1D/2D) shows relatively larger acceptor domains and a smaller intermixing domain, contributing to the higher electron mobility and less recombination, which improves J_{SC}, FF, and PCE. **J71** and **ITIC1** show better miscibility relative to **FTAZ** and **ITIC1**, which is beneficial to efficient charge generation and balanced charge transport, and thus higher J_{SC} and FF. Finally, the extra miscibility between **J71** and **ITIC2** leads to the largest intermixing domain size and thus more recombination and lower performance.

Table 3 Domain sizes calculated from GISAXS

	Intermixing (nm)	Acceptor (nm)	**FTAZ** (nm)
FTAZ:**ITIC1**	26.2	21.0	4.26
FTAZ:**ITIC2**	24.4	22.0	4.48
J71:**ITIC1**	30.7	5.74	—
J71:**ITIC2**	36.3	7.14	—

Conclusions

In summary, we choose two polymer donors with the same molecular backbone, **FTAZ** and **J71**, and two nonfullerene acceptors with the same molecular backbone, **ITIC1** and **ITIC2**, to investigate the effects of conjugation dimension (1D and 2D) on the performance of OSCs. **FTAZ** and **ITIC1** have 1D conjugation (*i.e.* only along backbone), while **J71** and **ITIC2** have 2D conjugation due to conjugated thienyl side chains. By pairing each of the different donors and acceptors together, a better understanding of the 1D/2D conjugation effect can be illustrated. First, 2D conjugated side chains slightly red-shift the absorption spectra and lower the bandgap for both the donor and acceptor materials. **J71** (2D) exhibits lower LUMO energy levels relative to **FTAZ** (1D) due to the σ inductive effect of silicon atoms on thienyl substituents, while **ITIC2** (2D) shows higher LUMO energy levels relative to **ITIC1** (1D) owing to the electron-donating property of thienyl side chains. Furthermore, 2D conjugated side chains on the acceptor induce self-aggregation of the small molecule acceptors, leading to larger acceptor domain size. Conjugated side chains on the polymer donor improve the miscibility of the donor and acceptor, and thus increase the intermixing domain size. Large pure domain facilitates charge transport but restrains exciton splitting, while large intermixing domain is beneficial to exciton splitting but unfavorable to charge transport. Additionally, the 2D conjugated side chain can effectively adjust the crystallinity and miscibility of donors and acceptors simultaneously, thus reaching a balance between charge transport and exciton dissociation, and finally achieving better performance. In this work, the combinations of 1D donor/2D acceptor (**FTAZ**/**ITIC2**) and 2D donor/1D acceptor (**J71**/**ITIC1**) achieve balance relative to the 1D/1D and 2D/2D blends, thus showing higher PCEs. Therefore, this work suggests that pairing mixed conjugation systems (*i.e.* 1D and 2D) might be a technique to achieve higher efficiency in OSCs.

Conflicts of interest

The authors declare no conflict of interest.

Acknowledgements

X. Z. thanks the National Natural Science Foundation of China (Grant No. 51761165023 and 21734001). X. L. thanks NSFC/RGC Joint Research Scheme No. N_CUHK418/17 and the financial support from Research Grant Council of Hong Kong (General Research Fund No. 14314216 and Theme-based Research Scheme No. T23-407/13-N). J. R. and W. Y. were supported by a NSF grant (CBET-1639429).

Notes and references

1 G. Li, R. Zhu and Y. Yang, *Nat. Photonics*, 2012, **6**, 153.
2 F. C. Krebs, N. Espinosa, M. Hösel, R. R. Søndergaard and M. Jørgensen, *Adv. Mater.*, 2014, **26**, 29–39.
3 L. Lu, T. Zheng, Q. Wu, A. M. Schneider, D. Zhao and L. Yu, *Chem. Rev.*, 2015, **115**, 12666–12731.
4 G. Yu, J. Gao, J. C. Hummelen, F. Wudl and A. J. Heeger, *Science*, 1995, **270**, 1789–1791.
5 J. J. M. Halls, C. A. Walsh, N. C. Greenham, E. A. Marseglia, R. H. Friend, S. C. Moratti and A. B. Holmes, *Nature*, 1995, **376**, 498–500.
6 Y. Li and Y. Zou, *Adv. Mater.*, 2008, **20**, 2952–2958.
7 L. Ye, S. Zhang, L. Huo, M. Zhang and J. Hou, *Acc. Chem. Res.*, 2014, **47**, 1595–1603.
8 L. Dou, Y. Liu, Z. Hong, G. Li and Y. Yang, *Chem. Rev.*, 2015, **115**, 12633–12665.
9 H. Yao, L. Ye, H. Zhang, S. Li, S. Zhang and J. Hou, *Chem. Rev.*, 2016, **116**, 7397–7457.
10 K. Feng, G. Yang, X. Xu, G. Zhang, H. Yan, O. Awartani, L. Ye, H. Ade, Y. Li and Q. Peng, *Adv. Energy Mater.*, 2018, **8**, 1602773.
11 J. Wang, W. Wang, X. Wang, Y. Wu, Q. Zhang, C. Yan, W. Ma, W. You and X. Zhan, *Adv. Mater.*, 2017, **29**, 1702125.
12 J. Wang, J. Zhang, Y. Xiao, T. Xiao, R. Zhu, C. Yan, Y. Fu, G. Lu, X. Lu, S. R. Marder and X. Zhan, *J. Am. Chem. Soc.*, 2018, **140**, 9140–9147.
13 C. Yan, S. Barlow, Z. Wang, H. Yan, A. K. Y. Jen, S. R. Marder and X. Zhan, *Nat. Rev. Mater.*, 2018, **3**, 18003.
14 P. Cheng, G. Li, X. Zhan and Y. Yang, *Nat. Photonics*, 2018, **12**, 131–142.
15 J. Hou, O. Inganäs, R. H. Friend and F. Gao, *Nat. Mater.*, 2018, **17**, 119–128.
16 G. Zhang, J. Zhao, P. C. Y. Chow, K. Jiang, J. Zhang, Z. Zhu, J. Zhang, F. Huang and H. Yan, *Chem. Rev.*, 2018, **118**, 3447–3507.
17 Y. Lin, J. Wang, Z.-G. Zhang, H. Bai, Y. Li, D. Zhu and X. Zhan, *Adv. Mater.*, 2015, **27**, 1170–1174.
18 Y. Lin and X. Zhan, *Adv. Energy Mater.*, 2015, **5**, 1501063.
19 L. Meng, Y. Zhang, X. Wan, C. Li, X. Zhang, Y. Wang, X. Ke, Z. Xiao, L. Ding, R. Xia, H.-L. Yip, Y. Cao and Y. Chen, *Science*, 2018, **361**, 1094–1098.
20 Y. Lin, F. Zhao, Y. Wu, K. Chen, Y. Xia, G. Li, S. K. K. Prasad, J. Zhu, L. Huo, H. Bin, Z.-G. Zhang, X. Guo, M. Zhang, Y. Sun, F. Gao, Z. Wei, W. Ma, C. Wang, J. Hodgkiss, Z. Bo, O. Inganäs, Y. Li and X. Zhan, *Adv. Mater.*, 2017, **29**, 1604155.
21 S. Chen, Y. An, G. K. Dutta, Y. Kim, Z.-G. Zhang, Y. Li and C. Yang, *Adv. Funct. Mater.*, 2017, **27**, 1603564.
22 S. Chen, H. J. Cho, J. Lee, Y. Yang, Z.-G. Zhang, Y. Li and C. Yang, *Adv. Energy Mater.*, 2017, **7**, 1701125.
23 M. Jeong, S. Chen, S. M. Lee, Z. Wang, Y. Yang, Z.-G. Zhang, C. Zhang, M. Xiao, Y. Li and C. Yang, *Adv. Energy Mater.*, 2017, **8**, 1702166.
24 S. Chen, S. M. Lee, J. Xu, J. Lee, K. Lee, T. Hou, Y. Yang, M. Jeong, B. Lee, Y. Cho, S. Jung, J. Oh, Z.-G. Zhang, C. Zhang, M. Xiao, Y. Li and C. Yang, *Energy Environ. Sci.*, 2018, **11**, 2569–2580.
25 Y. Qin, M. A. Uddin, Y. Chen, B. Jang, K. Zhao, Z. Zheng, R. Yu, T. J. Shin, H. Y. Woo and J. Hou, *Adv. Mater.*, 2016, **28**, 9416–9422.
26 S. Dai, F. Zhao, Q. Zhang, T.-K. Lau, T. Li, K. Liu, Q. Ling, C. Wang, X. Lu, W. You and X. Zhan, *J. Am. Chem. Soc.*, 2017, **139**, 1336–1343.
27 F. Zhao, S. Dai, Y. Wu, Q. Zhang, J. Wang, L. Jiang, Q. Ling, Z. Wei, W. Ma, W. You, C. Wang and X. Zhan, *Adv. Mater.*, 2017, **29**, 1700144.
28 J. Zhu, Z. Ke, Q. Zhang, J. Wang, S. Dai, Y. Wu, Y. Xu, Y. Lin, W. Ma, W. You and X. Zhan, *Adv. Mater.*, 2018, **30**, 1704713.
29 J.-D. Chen, Y.-Q. Li, J. Zhu, Q. Zhang, R.-P. Xu, C. Li, Y.-X. Zhang, J.-S. Huang, X. Zhan, W. You and J.-X. Tang, *Adv. Mater.*, 2018, **30**, 1706083.
30 C. Sun, F. Pan, H. Bin, J. Zhang, L. Xue, B. Qiu, Z. Wei, Z.-G. Zhang and Y. Li, *Nat. Commun.*, 2018, **9**, 743.
31 Y. Lin, F. Zhao, S. K. K. Prasad, J.-D. Chen, W. Cai, Q. Zhang, K. Chen, Y. Wu, W. Ma, F. Gao, J.-X. Tang, C. Wang, W. You, J. M. Hodgkiss and X. Zhan, *Adv. Mater.*, 2018, **30**, 1706363.
32 P. Cheng, J. Wang, Q. Zhang, W. Huang, J. Zhu, R. Wang, S. Y. Chang, P. Sun, L. Meng, H. Zhao, H. W. Cheng, T. Huang, Y. Liu, C. Wang, C. Zhu, W. You, X. Zhan and Y. Yang, *Adv. Mater.*, 2018, **30**, 1801501.
33 Y. Lin, Q. He, F. Zhao, L. Huo, J. Mai, X. Lu, C.-J. Su, T. Li, J. Wang, J. Zhu, Y. Sun, C. Wang and X. Zhan, *J. Am. Chem. Soc.*, 2016, **138**, 2973–2976.
34 Y. Lin, F. Zhao, Q. He, L. Huo, Y. Wu, T. C. Parker, W. Ma, Y. Sun, C. Wang, D. Zhu, A. J. Heeger, S. R. Marder and X. Zhan, *J. Am. Chem. Soc.*, 2016, **138**, 4955–4961.
35 H. Bin, L. Gao, Z.-G. Zhang, Y. Yang, Y. Zhang, C. Zhang, S. Chen, L. Xue, C. Yang, M. Xiao and Y. Li, *Nat. Commun.*, 2016, **7**, 13651.
36 B. Kan, H. Feng, X. Wan, F. Liu, X. Ke, Y. Wang, Y. Wang, H. Zhang, C. Li, J. Hou and Y. Chen, *J. Am. Chem. Soc.*, 2017, **139**, 4929–4934.
37 W. Wang, C. Yan, T.-K. Lau, J. Wang, K. Liu, Y. Fan, X. Lu and X. Zhan, *Adv. Mater.*, 2017, **29**, 1701308.
38 L. Xue, Y. Yang, J. Xu, C. Zhang, H. Bin, Z.-G. Zhang, B. Qiu, X. Li, C. Sun, L. Gao, J. Yao, X. Chen, Y. Yang, M. Xiao and Y. Li, *Adv. Mater.*, 2017, **29**, 1703344.
39 S. Xu, Z. Zhou, W. Liu, Z. Zhang, F. Liu, H. Yan and X. Zhu, *Adv. Mater.*, 2017, **29**, 1704510.
40 Y. Liu, Z. Zhang, S. Feng, M. Li, L. Wu, R. Hou, X. Xu, X. Chen and Z. Bo, *J. Am. Chem. Soc.*, 2017, **139**, 3356–3359.
41 Z. Xiao, X. Jia, D. Li, S. Wang, X. Geng, F. Liu, J. Chen, S. Yang, T. P. Russell and L. Ding, *Sci. Bull.*, 2017, **62**, 1494–1496.
42 T. Li, S. Dai, Z. Ke, L. Yang, J. Wang, C. Yan, W. Ma and X. Zhan, *Adv. Mater.*, 2018, **30**, 1705969.
43 J. Zhang, C. Yan, W. Wang, Y. Xiao, X. Lu, S. Barlow, T. C. Parker, X. Zhan and S. R. Marder, *Chem. Mater.*, 2018, **30**, 309–313.
44 J. Zhu, Y. Xiao, J. Wang, K. Liu, H. Jiang, Y. Lin, X. Lu and X. Zhan, *Chem. Mater.*, 2018, **30**, 4150–4156.

45 W. Liu, J. Zhang, Z. Zhou, D. Zhang, Y. Zhang, S. Xu and X. Zhu, *Adv. Mater.*, 2018, **30**, 1800403.

46 S. Zhang, Y. Qin, J. Zhu and J. Hou, *Adv. Mater.*, 2018, **30**, 1800868.

47 S. Li, L. Ye, W. Zhao, H. Yan, B. Yang, D. Liu, W. Li, H. Ade and J. Hou, *J. Am. Chem. Soc.*, 2018, **140**, 7159–7167.

48 Z. Luo, H. Bin, T. Liu, Z.-G. Zhang, Y. Yang, C. Zhong, B. Qiu, G. Li, W. Gao, D. Xie, K. Wu, Y. Sun, F. Liu, Y. Li and C. Yang, *Adv. Mater.*, 2018, **30**, 1706124.

49 Y. Xie, F. Yang, Y. Li, M. A. Uddin, P. Bi, B. Fan, Y. Cai, X. Hao, H. Y. Woo, W. Li, F. Liu and Y. Sun, *Adv. Mater.*, 2018, **30**, 1803045.

50 Y. Zhang, B. Kan, Y. Sun, Y. Wang, R. Xia, X. Ke, Y. Q. Q. Yi, C. Li, H. L. Yip, X. Wan, Y. Cao and Y. Chen, *Adv. Mater.*, 2018, **30**, 1707508.

51 S. Dai, T. Li, W. Wang, Y. Xiao, T.-K. Lau, Z. Li, K. Liu, X. Lu and X. Zhan, *Adv. Mater.*, 2018, **30**, 1706571.

52 X. Xu, Z. Li, Z. Bi, T. Yu, W. Ma, K. Feng, Y. Li and Q. Peng, *Adv. Mater.*, 2018, **30**, 1800737.

53 Z. Li, X. Xu, G. Zhang, T. Yu, Y. Li and Q. Peng, *Sol. RRL*, 2018, **2**, 1800186.

54 Q. An, W. Gao, F. Zhang, J. Wang, M. Zhang, K. Wu, X. Ma, Z. Hu, C. Jiao and C. Yang, *J. Mater. Chem. A*, 2018, **6**, 2468–2475.

55 S. C. Price, A. C. Stuart, L. Yang, H. Zhou and W. You, *J. Am. Chem. Soc.*, 2011, **133**, 4625–4631.

56 J. Pommerehne, H. Vestweber, W. Guss, R. F. Mahrt, H. Bassler, M. Porsch and J. Daub, *Adv. Mater.*, 1995, **7**, 551–554.

57 J. Ohshita, *Macromol. Chem. Phys.*, 2009, **210**, 1360–1370.

58 G. G. Malliaras, J. R. Salem, P. J. Brock and C. Scott, *Phys. Rev. B: Condens. Matter Mater. Phys.*, 1998, **58**, 13411–13414.

59 B. Ray, M. S. Lundstrom and M. A. Alam, *Appl. Phys. Lett.*, 2012, **100**, 013307.

60 Z. Tang, J. Wang, A. Melianas, Y. Wu, R. Kroon, W. Li, W. Ma, M. R. Andersson, Z. Ma, W. Cai, W. Tress and O. Inganäs, *J. Mater. Chem. A*, 2018, **6**, 12574–12581.

61 L. J. A. Koster, V. D. Mihailetchi, R. Ramaker and P. W. M. Blom, *Appl. Phys. Lett.*, 2005, **86**, 123509.

62 S. R. Cowan, A. Roy and A. J. Heeger, *Phys. Rev. B: Condens. Matter Mater. Phys.*, 2010, **82**, 245207.

63 S. Wheeler, F. Deledalle, N. Tokmoldin, T. Kirchartz, J. Nelson and J. R. Durrant, *Phys. Rev. Appl.*, 2015, **4**, 024020.

64 S. Solak, P. W. M. Blom and G. A. H. Wetzelaer, *Appl. Phys. Lett.*, 2016, **109**, 053302.

65 I. Riedel, J. Parisi, V. Dyakonov, L. Lutsen, D. Vanderzande and J. C. Hummelen, *Adv. Funct. Mater.*, 2004, **14**, 38–44.

66 M. A. Faist, S. Shoaee, S. Tuladhar, G. F. A. Dibb, S. Foster, W. Gong, T. Kirchartz, D. D. C. Bradley, J. R. Durrant and J. Nelson, *Adv. Energy Mater.*, 2013, **3**, 744–752.

67 J. Mai, Y. Xiao, G. Zhou, J. Wang, J. Zhu, N. Zhao, X. Zhan and X. Lu, *Adv. Mater.*, 2018, **30**, 1802888.

68 L. Ye, B. A. Collins, X. Jiao, J. Zhao, H. Yan and H. Ade, *Adv. Energy Mater.*, 2018, **8**, 1703058.

69 L. Ye, H. Hu, M. Ghasemi, T. Wang, B. A. Collins, J.-H. Kim, K. Jiang, J. H. Carpenter, H. Li, Z. Li, T. McAfee, J. Zhao, X. Chen, J. L. Y. Lai, T. Ma, J.-L. Bredas, H. Yan and H. Ade, *Nat. Mater.*, 2018, **17**, 253–260.

70 J. Mai, T.-K. Lau, J. Li, S.-H. Peng, C.-S. Hsu, U. S. Jeng, J. Zeng, N. Zhao, X. Xiao and X. Lu, *Chem. Mater.*, 2016, **28**, 6186–6195.